JMEPEG (2005) 14:487-494
DOI: 10.1361/105994905X56188

1059-9495/$19.00

Advanced High-Velocity Oxygen-Fuel Coating and Candidate Materials for Protecting LP Steam Turbine Blades Against Droplet Erosion

B.S. Mann, Vivek Arya, and Pankaj Joshi

(Submitted September 9, 2004; in revised form May 31, 2005)

This paper describes the water droplet erosion characteristics of advanced high-velocity oxygen-fuel (HVOF) coating and the materials used for steam turbine blading. For droplet erosion study, round samples as per ASTM G73-98 ("Standard Practice for Liquid Impingement Erosion Testing," Vol 03.02, *Annual Book of ASTM Standards,* ASTM, 2004) were selected. The materials commonly used for steam turbine blading are X20Cr13, X10CrNiMoV122, and Ti6Al4V. During incubation as well as in the long run, advanced HVOF coating has performed much better than all these materials. This is due to enhanced particle kinetic energy caused by optimum flow of oxygen and fuel injection by modifying the fuel injector. Droplet erosion test results of these materials and advanced HVOF coating along with their properties and damage mechanism are reported and discussed in this paper.

Keywords droplet erosion, HVOF coating, steam turbine, titanium alloy

1. Introduction

Water droplet erosion is a well-known phenomenon occurring on the moving blades operating at the low-pressure end of steam turbines. This is initiated by "small" primary droplet condensate in bulk of the supercooled steam in the flow, which becomes separated on the blade surface and generates secondary "large" droplets, causing erosion. Relatively large drops, up to 800 μm diameter, are consistently produced and accelerated and strike on the convex side of the moving blades. The water drops greater than 200 μm and a terminal velocity more than 250 m/s are responsible for quick erosion. Material loss from the leading edge is the result of commutative damage from the impact of water droplets. The impact of large droplets 800 μm at 300 m/s generates high local forces. The damage produced by one or more of these loading conditions on a material surface exposed to single or multiple water drop impact is responsible for initiating damage and subsequent material removal (Ref 1-10). The evaluation of damage produced in target material caused by the single water drop loading cycle is a complex dynamic process. Recently, high-velocity oxygen-fuel (HVOF) coatings and laser hardening have proved to be the best candidate materials for water droplet erosion resistance (Ref 10). It has been reported that laser hardening is an excellent shield for this application; however, it introduces both compressive as well as tensile residual stresses in the steel (Ref 11-13). Austenite phase retention resulting in volume decrease gives rise to the tensile stresses, whereas martensite transformation causes volume increase and gives rise to compressive residual stresses. The distribution of these stresses largely depends upon heating and cooling rates of the laser-hardened layer. The thin edges of the low pressure steam turbine (LPST) blades undergo convex bending in the longitudinal direction, causing reduction in tensile stresses. On the other hand, the blades suffer a considerably smaller deformation or even a slight concave bending, which causes an increase in tensile residual stresses. Thus, the residual stresses in laser hardened layer in the longitudinal direction are compressive and generally range between 5 and 80 MPa, whereas in the transition area from the hardened layer to matrix, they change into tensile residual stresses. In the transverse direction, the residual stresses are always tensile and range from 50 to 200 MPa. The tensile stresses on the laser-hardening surface may initiate cracks that may propagate into the blade material causing failure. On the other hand, for the HVOF coatings, these stresses are compressive in nature due to peening action of the high velocity oxyfuel spray coatings as the particles travel at the rate of more than 600-700 m/s. For the HVOF processes studied so far, the depth of peening effects could be as much as 50 μm and may be much more for heavier tungsten carbide powders as the intensity of the peening is directly proportional to the mass and square of the particle velocity ($1/2\ mv^2$). These compressive stresses range from 200 to 400 MPa (Ref 14). These are highly beneficial to arrest the initiation of the cracks and minimize the breakage of the LPST blades avoiding unnecessary outages. Therefore, the process becomes very attractive for steam turbine blading. Advanced coating such as plasma assisted chemical vapor deposition (PACVD), super D-Gun LW45 (WC10Co4Cr), have been studied for corrosive and erosive oil field gate valve application (Ref 15). Because WC10Co4Cr is a reasonably good material, it can be deposited by high-velocity oxyfuel sprayed technique and has recently been studied for this application (Ref 10). For the current study, the conventional spray gun of HVOF system was upgraded by modifying the fuel injection and enhancing the fuel atomizing process. The atomization process is based upon the multipoint fuel injection concept, which completely burns the carbon in the liquid fuel producing extra energy. This helps in further acceleration of

B.S. Mann, Vivek Arya, and **Pankaj Joshi,** Surface Coatings and Treatment Laboratory, BHEL, Corporate R&D Division, Vikasnagar, Hyderabad-500093, India. Contact e-mail: balbir@bhelrnd.co.in.

carbide particles in the HVOF flame producing a dense cohesive and well-bonded layer. The process of fuel atomization to produce well-bonded and cohesive HVOF coating, along with droplet erosion resistance of all these materials, is reported in this paper.

2. Energy Flux

The energy flux of the water droplet is associated with normal component of the droplet impact velocity w^*N (r^*,η), the droplet size defined by r^*, and the blade surface element $d\eta$ $\Delta R_1/\sin\beta_{b1}$, (η) at η is given by (Ref 3, 4):

$$\delta E_k = \frac{n(r^*)^3}{4\pi(r^*)^3 \rho^* \frac{w^*}{2} N^3(r^*, \eta)} \frac{d\eta}{\sin\beta_{b1}(\eta)}$$

The total amount of energy transferred by all the droplets to the surface under consideration is:

$$dE_k(\eta) = \sum_{r^*=r^*_{min}}^{r^*(\eta)} \delta E_k(r^*, \eta), \left(\frac{J}{s}\right)$$

The energy flux is given by:

$$E_k(\eta) = \frac{d\,E_k\,(\eta)}{d\eta \Delta R_1} \sin\beta_{b1}(\eta), \left(\frac{J}{m^2 s}\right)$$

$$= \frac{\Delta M^*}{\Delta R_1} \frac{1}{t_w} \left(\frac{1}{\int_0^\infty w^* ax(r^*, \eta = 0)(r^*)^3 f_n(r^*) dr^*} \right)$$

$$\frac{1}{2} \int_{r^*_{min}}^{r^*(\eta)} w^* N^3(r^*, \eta)(r^*)^3 f_n(r^*) dr^*$$

$$= \frac{\Delta M^*}{\Delta R_1} EK(\eta)$$

where t_w is the rotor blade spacing (m), $\Delta M^*/\Delta R_1$ is the total amount of water entering over length ΔR_1 (kg/s), r^* is the droplet radius (m), $w^*N(\eta)$ is the maximum value of the normal components of impact velocity (m/s), w^*_{ax} is the axial velocity of the droplet velocity (m/s), $R^*(\eta)$ is the maximum droplet radius (m), N is the perpendicular distance from the leading edge, f_n is the number distribution, R is the distance of the blade profile from the axis of the rotor (m), η is a coordinate (m), and β_{b1} is the blade tangent inclination (degrees).

The water droplet energy flux in the last stage of a moving steam turbine blade for a particular profile in 200 MW plant is given in Fig. 1 (Ref 3, 4). These values lie in the range of 4×10^6 to 15×10^6 J/m^{2}s. The energy flux for four different water droplet sizes, i.e., 213, 109, 78, and 49 μm, is plotted in Fig. 1. The figure shows that energy flux in the region of the leading edge rises exponentially, close to 15×10^6 J/m^{2}s, and this can be higher for a larger water droplet. The droplet erosion tests were conducted at 29.9×10^6 J/m^{2}s to obtain results in short duration tests.

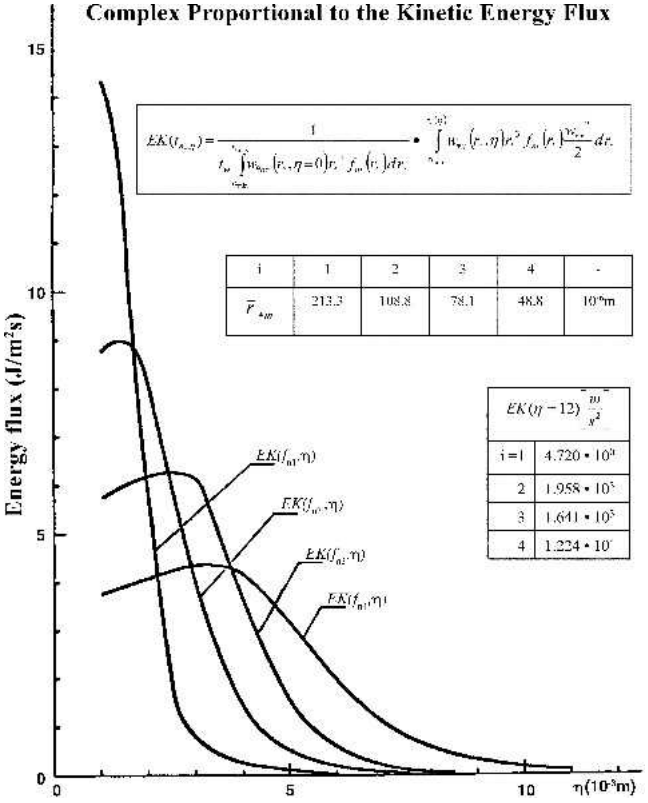

Fig. 1 Energy flux of 200 Mw LPST blade (Ref 3)

2.1 Corrosion Aspects

Fatigue, along with droplet erosion, is considered to be the most common single factor of LPST blade failure. Corrosion alone is not considered a contributing factor. This was also experienced at a number of sites that have run for more than 15 years. The formation of pits due to droplet erosion at a critical location on a turbine blade may aggravate cracking of the blade in two ways: as a stress concentration, causing the blade to experience high stresses (both static and cyclic), and as a stagnant corrosion cell, where the environment at the base of the pit can change concentration as corrosion proceeds. The latter situation can lead to a low pH and more acidic environment, which is known to be deleterious to the corrosion fatigue life of conventional blading alloys. However, the pH values in power plants are usually maintained within normal limits, so this situation rarely arises.

Corrosion testing of all the materials generally used for steam turbine blading, along with advanced HVOF coatings for durations up to 100 h, was done as per ASTM B-117-73 (Ref 16). The test results are based on the physical observation of the samples for different times. Corrosion initiation and rust formation and stain appearance have been used to compare corrosion results. The corrosion of the HVOF coating is comparable to X20Cr13 steel. The corrosion of heat-treated X10CrNiMoV122 steel is inferior to the nonheat treated steel because the retained austenite has converted to martensite and is sensitive to the chlorides in the salt. Silica and/or chloride deposits, which are common in steam turbines, aggravate stress corrosion cracking. The initiation of corrosion damage for durations up to 24 h on these materials is shown in Fig. 2. The trend in damage continued for durations up to 100 h. Figure 2 shows that Ti6Al4V and SS321 are free from any attack. These

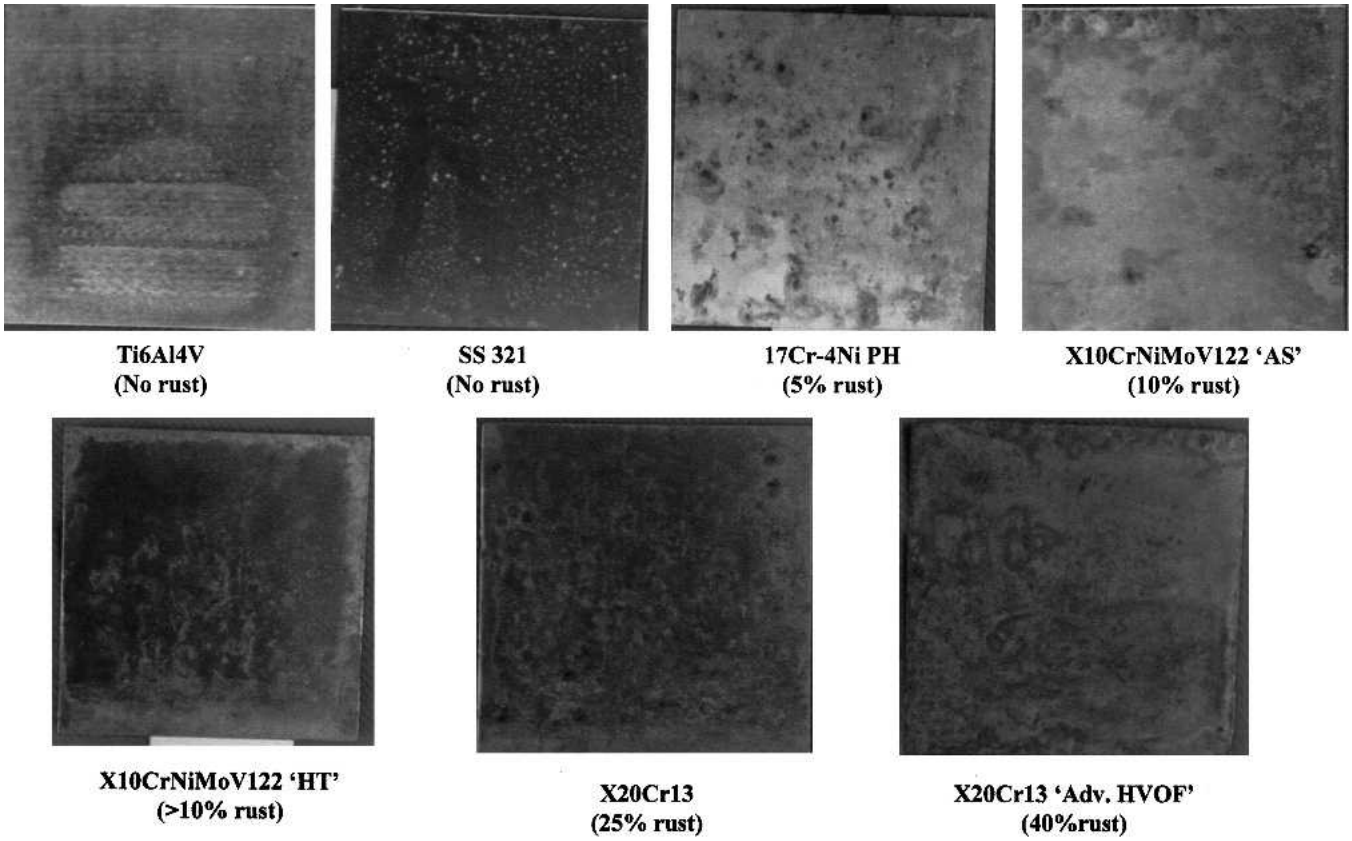

Fig. 2 Salt spray test on various materials (damages in ascending order)

two alloys are followed by 17Cr-4NiPH, X10CrNiMoV122 (AS), X10CrNiMoV122 (HT), X20Cr13 (AS), and the HVOF coating.

2.2 Fracture Toughness

The fracture toughness of the surface coating plays a significant role in the droplet erosion resistance. The fracture toughness (k_{1c}) of the advanced HVOF coating was evaluated using the surface indentation technique. A load of 30 kg was applied, and the indent diagonal (a) and crack length (c) were measured (Ref 17). The advanced HVOF coating produced by the modified fuel injector did not show any cracking, whereas the coating processed using the conventional injector was cracked. Figures 3(a) and (b) show the indents on the HVOF coating. The conventional k_{1c} value lies in the range of 4-5 MPa$\sqrt{m}$. The coatings deposited with the modified injector did not show any cracking so their fracture toughness values could not be determined. These results suggest that a significant improvement in fracture toughness has been achieved and is caused by the complete combustion of the fuel, as there is absolutely no sign of residual carbon in the HVOF flame. The flame using the modified injector is very sharp and concentrated, whereas the flame when using the conventional injector is broad and diffuse.

3. HVOF Coatings

WC powders are widely used to produce dense, high hardness, wear-resistant coatings, especially to combat erosion and corrosion (Ref 18). WC-Co, using either Ni or Cr, is typically used with WC-Co-Cr powders preferred when corrosion resistance is needed.

The HVOF coatings are based on liquid as well as gaseous fuel. The liquid fuel systems are preferred due to ease of operation and safety. These systems have the limitations of complete combustion of the hydrocarbons in the liquid fuel (such as kerosene and diesel). The complete combustion of hydrocarbons in the liquid fuel depends upon the atomization of the fuel and proper mixing of the fuel and oxygen. Diesel fuel and aviation kerosene have excessive aromatics requiring smaller fuel droplets for complete combustion. These depend upon the numbers of fuel injection points and their spacing and location. The conventional fuel injector has a limited number of fuel injection points (i.e., three fuel injection points), leading to excessive unburned carbon in the HVOF flame. In the current study, the number of fuel injection points was increased to eight. The coatings obtained with the modified injector were evaluated for droplet erosion resistance. Samples ϕ12.7 × 40 mm in length were coated using the HVOF automatic mode. Air cooling was used so the temperature of the samples was maintained below 125 °C. Coating thickness was 250 ± 30 μm for all samples.

4. Water Droplet Erosion Testing of Different Coatings

The details of erosion test facility are given in Ref 10. In short, the test facility consists of a 700 mm diameter chamber and a round disk on which the test samples are positioned.

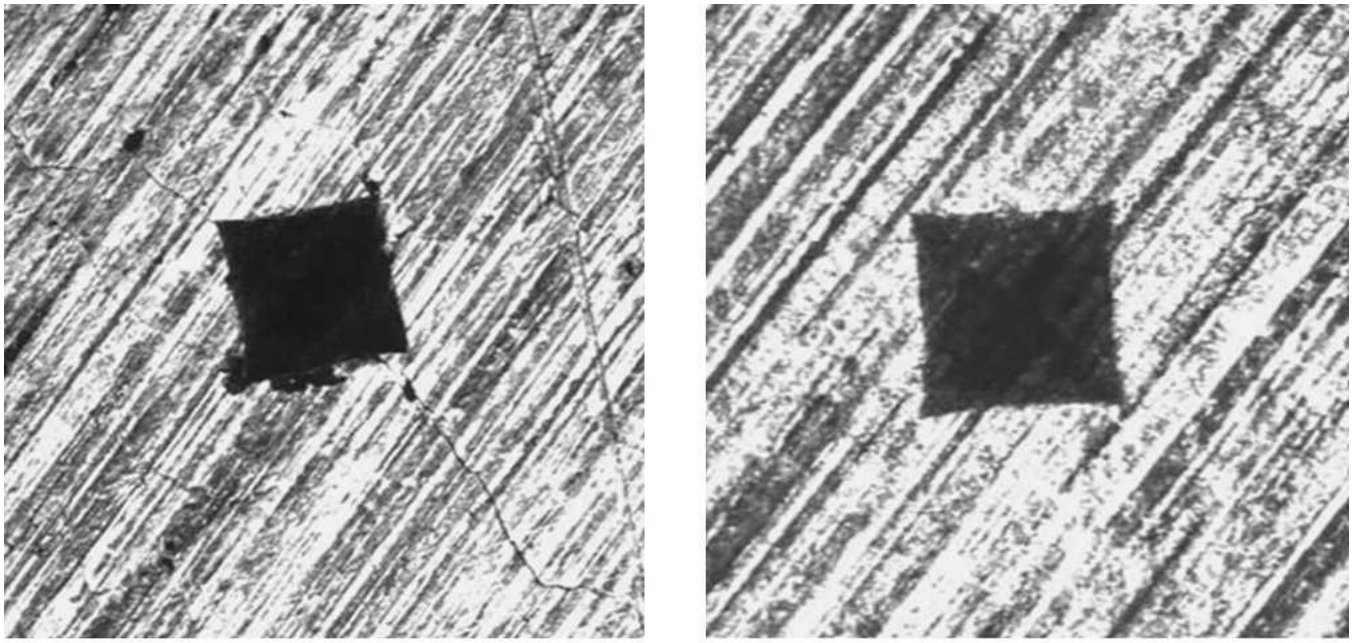

(a) (b)

Fig. 3 Surface indentation of a conventional and advanced HVOF coated X20Cr13 steel: (a) convention HVOF showing deep diagonal cracks and (b) advanced HVOF showing no cracks

Samples 40 mm in length and 12.7 mm in diameter are affixed on the periphery of the disk. As such, a relative velocity of 147.6 m/s can be attained. A precision balance (±0.1 mg) was used for measurement of mass loss after testing. The test duration was selected to achieve steady state impingement. The accuracy of the test results were confirmed using 321SS as a reference material. The deviation and accuracy of the mass loss measurements for the test apparatus lie within the specified range established from different laboratories (Ref 19). The results were plotted in the form of a cumulative erosion rate-time curve. The extent of erosion damage is calculated from the mass loss divided by the density of the coatings and/or alloy. Table 1 gives the materials tested for droplet erosion. Test conditions are given in Table 2.

5. Results and Discussion

5.1 Properties of Materials and Coatings

Tables 3 and 4 give the mechanical properties of all materials and coatings. As mentioned previously, the property that correlates well with erosion resistance is the "modified resilience." This can be seen from Fig. 4 and 5 and Tables 4 and 5. Other properties such as toughness and yield strength do not appear to correlate as well with erosion behavior. The basic mechanical properties along with droplet erosion resistance of conventional HVOF coatings have already been reported (Ref 10).

5.2 Microhardness

The microhardness and hardness of the coated and uncoated steels were measured using a load of 10 kg. The hardness values are given in Table 3. The microhardness of the advanced HVOF coating has increased significantly (i.e., 1500 H_v in comparison to 1200 H_v for the conventional injector).

Table 1 Various materials used for droplet erosion testing

Materials	Composition, wt.%
SS321	0.048C, 0.58Si, 1.57Mn, 17Cr, 13.5Ni, 2.39Mo, 0.5Ti, Bal. Fe
X20Cr13	0.20C, 0.5Si, 0.5Mn, 13Cr, 0.5Ni,, Bal. Fe
X10CrNiMoV122	0.1C, 0.25Si, 0.7Mn, 12Cr, 2.5Ni, 1.75Mo, 0.3V, Bal. Fe
17Cr-4Ni PH	0.06C, 15.67Cr, 0.27Si, 0.64Mn, 4.25Ni, 3.6Cu, 0.19Nb, Bal. Fe

Table 2 Experimental test conditions

Conditions	Test II
Water jet size	3.2×10^{-3} m
Water energy flux	29.88×10^6 J/m^{2}s
Relative water velocity	147.6 m/s
Test sample size	φ 12.70 × 40 mm
Water droplet dize	100-300 μm
Number of specimens used	12
Test duration	10.98×10^6 cycles (N)
Jet distance	100 mm
Angle of impingement	0-90°
Impact frequency	78 cycles/s
Experimental accuracy	±17.5%

5.3 Droplet Erosion Test

The droplet erosion test results of different stainless steels and Ti6Al4V along with the advanced HVOF coating are shown in Fig. 4 and 5. It can be seen that excellent performance is achieved by the advanced HVOF coating followed by Ti6Al4V, 17Cr-4Ni PH, and X10CrNiMoV122 steel. It can also be seen that the HVOF-coated WC10Co4Cr steel per-

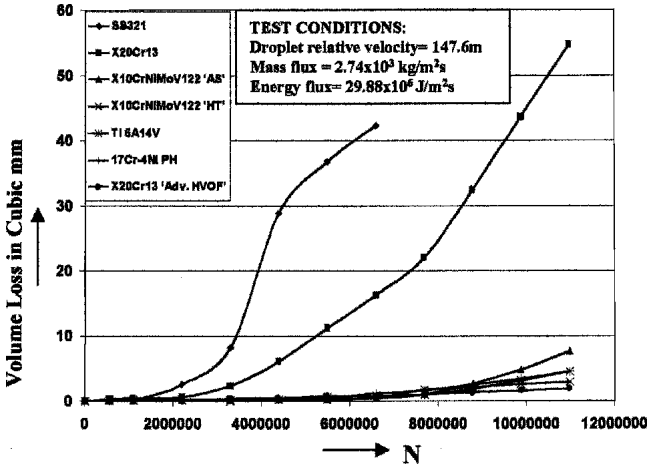

Fig. 4 Volume loss of different materials and coatings at an energy flux of 29.88×10^6 J/m^{2}s

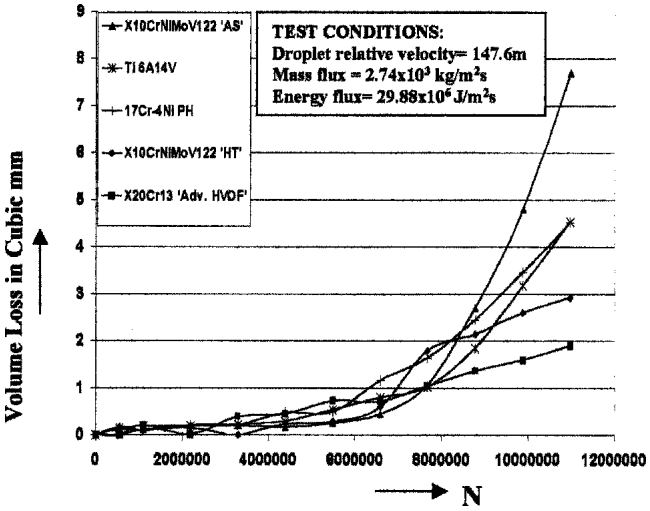

Fig. 5 Volume loss of different materials and coatings at an energy flux of 29.88×10^6 J/m^{2}s

Table 3 Mechanical properties of different coatings and materials

Materials/coatings materials	YS, N/mm^2	UTS, N/mm^2	Hardness, HV	EL, %	Ultimate resilience, J/cm^3	Strain energy, J/cm^3	Impact strength, J
SS321	390	837	135-145	48.4	1.67	328	355
X20Cr13	721	876	300-350	23.2	1.83	164	93
X10CrNiMoV122 (AS)	857	1000	290-300	21.1	2.42	171	>100
17Cr-4Ni PH	863	1224	365-380	13.4	3.58	140	112
Ti6A14V	850	874	330-350	13.0	3.17	96	65
X20Cr13 (Adv. HVOF)	…	…	1450-1500	…	…	…	…

Note: UTS^2/2E, Ultimate resilience; UTS, ultimate tensile strength; E, Young's modulus; X20Cr13, actual steam turbine blade material in a forged condition; X10CrNiMoV122 'AS', actual steam turbine blade material in a forged condition; 17Cr-4Ni PH in as-cast condition; Ti6A14V in forged condition and later heat-treated for 1 h at 950 °C followed by water quench and aged for 6 h at 535 °C, X10CrNiMoV122 'HT', austenized for ½ h at 1000 °C followed by oil quench, hardness increased from 290-300 to 420-430 H_v

Table 4 Experimentally determined properties of different materials

Materials	Hardness, HV	Modified resilience, HV	Impact strength, J
SS321	135-145	0.310	355
X20Cr13	300-350	0.712	93.0
X10CrNiMoV122 (AS)	290-300	0.819	>100
17Cr-4Ni PH	365-380	1.13	112.0
Ti6A14V	330-350	1.29	65
X20Cr13 (Adv. HVOF)	1450-1500	3.54	…

$$\text{Modified resilience} = \frac{\text{UTS}_{\text{substrate}} \times \text{Hardness}_{\text{substrate/coating}}}{2E}$$

Table 5 Volume loss and ranking of different coatings/materials after 10.98×10^6 cycles (N) at 29.88×10^6 J/m^{2}s

Coating/materials	Ranking	Volume loss, mm^3
SS321	7	42.3(a)
X20Cr13	6	54.8
X10CrNiMoV122 (AS)	5	7.7
17Cr-4Ni PH	4	4.5
Ti6A14V	3	4.5
X10CrNiMoV122 (HT)	2	2.93
X20Cr13 (Adv. HVOF)	1	1.91

(a) Due to excessive wear out, the SS321 steel samples could not be continued after 6.8625×10^6 cycles (N).

formed much better, even during the incubation period. Relative ranking of the coatings and materials are given in Table 5. The superior performance of the advanced HVOF coating is caused by its high hardness and excellent toughness (lack of cracking during indentation testing) compared with the conventional HVOF coating. It is well known that physical properties of coated materials, such as tensile strength, modified resilience, binding energy and crystal structure, play a crucial role in determining the erosion resistance (Ref 10). It has also been observed that the higher the crystal binding energy of a material, the longer is the incubation period (Ref 20). However, the integrity of the coating, together with proper bonding to the substrate, along with crack resistance, play significant roles in the erosion resistance. Diffuse coatings can be produced by chemical vapour deposition and lead to composite structures (Ref 21). The excellent impingement erosion resistance of ad-

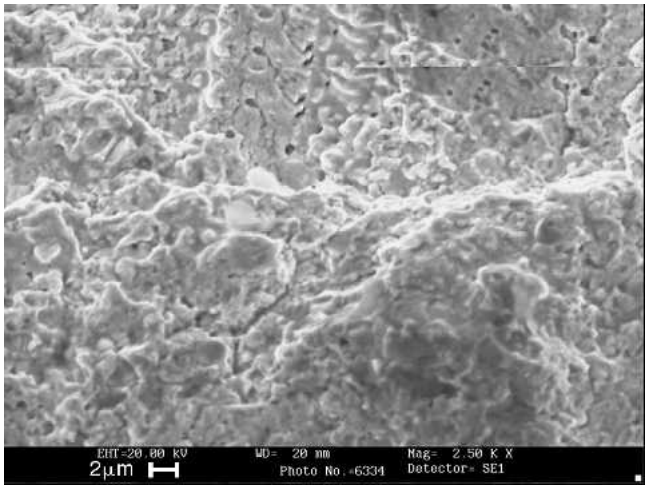

Fig. 6 SEM of eroded X20Cr13 (Adv. HVOF) showing coating is free from oxides and pores

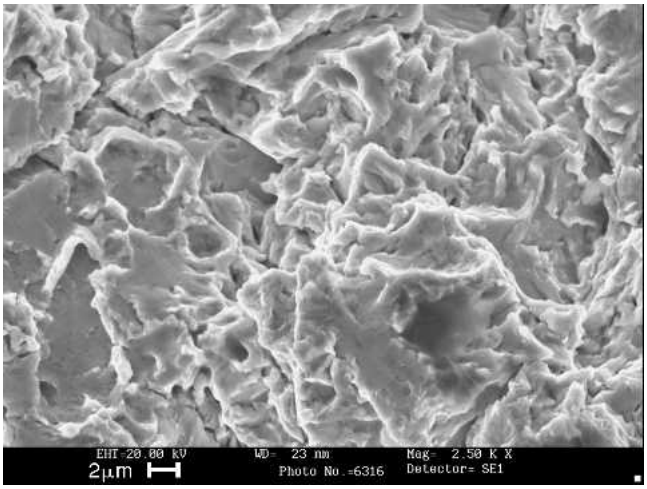

Fig. 8 SEM of eroded X10CrNiMoV122 (HT) showing tunnel type damages

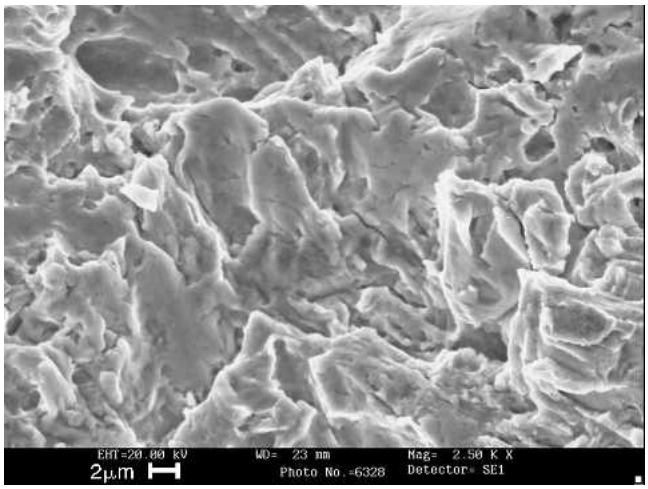

Fig. 7 SEM of eroded X10CrNiMoV122 (AS) showing deep erosion across the grains

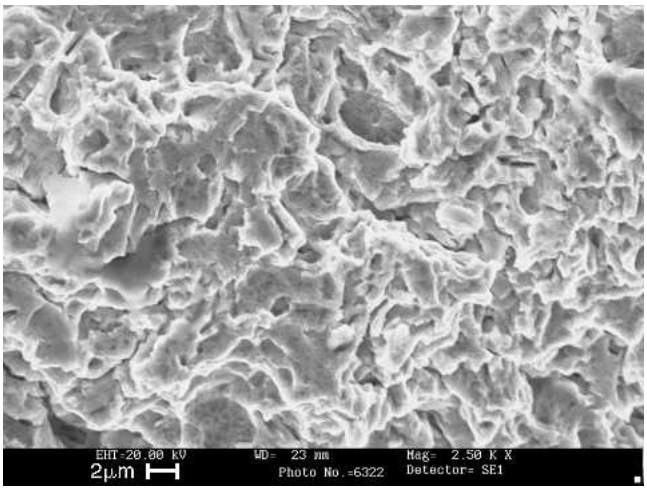

Fig. 9 SEM of eroded 17Cr-4Ni PH showing fine microstructure

vanced HVOF coatings can be explained on the basis that microjets formed by dividing bigger jets into smaller jets cannot penetrate the hard WC particles easily or break the matrix as it is very tough. The HVOF coating phenomenon is similar to cold welding. Kuroda et al. (Ref 14) have reported that compressive stresses ranging from 70 to 420 MPa were generated during HVOF spraying due to the peening effect of spraying particles in a semimolten state at high velocity. Compressive stresses on the order of 200 MPa in HVOF coatings exist to a 50 μm depth inside the substrate (Ref 14). These compressive stresses are likely to increase with increased kinetic energy of the sprayed particles in the case of the advanced fuel injection system used in this research. These compressive residual stresses are highly beneficial in reducing stress corrosion related fatigue damage and have improved performance.

5.4 Scanning Electron Microscopy

The mode of material removal in 17Cr-4Ni PH steel is across the grains, whereas in the case of Ti6Al4V, deep cavities are observed in the longitudinal direction (across the flow). The micrographs of erosion damage are shown in Fig. 6-9. The micrographs show that the microstructure of X10CrNiMoV122 is coarser than that of 17Cr-4Ni PH and becomes finer after heat treatment. Material removal is across the grain and similar in mode to other steels. The microstructure of the advanced HVOF coating is free from pores and very fine (Fig. 6). The microstructure details of the conventional HVOF coating have already been reported (Ref 10). Droplet eroded samples, tested according to ASTM G-73-98, are shown in Fig. 10. The samples have been arranged in decreasing order of the damage. A cross-sectional view of the test facility, which was designed and fabricated according to ASTM G-73-98, is shown in Fig. 11.

5.5 Field Experience

Droplet erosion damage of LPST blades has been experienced at a number of sites. The damage is visible only after many hours of operation (minimum operation of 15-20 years). The eroded blade from one of the sites is shown in Fig. 12. It

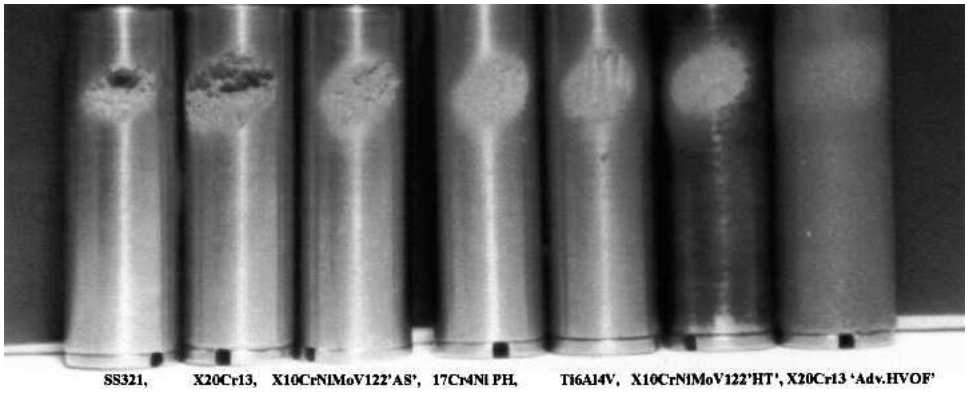

Fig. 10 Droplet eroded samples arranged in decreasing order of their damages

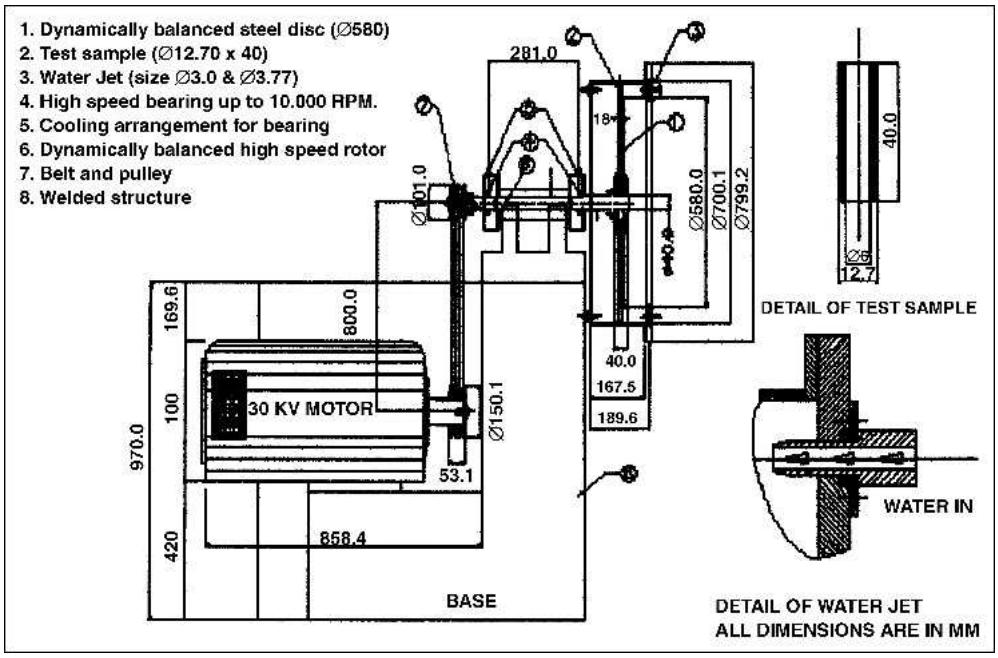

Fig. 11 Cross-sectional view of droplet erosion test ring

can be seen that corrosion alone does not appear to be a contributing factor. Only a few spots of rusting were observed (corrosion damage can, however, be easily removed by erosion damage). The corrosion resistance of advanced HVOF coating is comparable to that of X20Cr13 steel and may be slightly less. So, in the long run the HVOF coating is the right choice for protecting LPST blades against droplet erosion.

6. Conclusions

In droplet erosion, the advanced HVOF coating performed best from among the materials tested (SS321, X20Cr13, 17Cr-4Ni PH, X10CrNiMoV122, and Ti6Al4V). This technique, because of its enhanced kinetic energy, has the advantage of introducing additional compressive residual stresses within the coatings as well as in the base material. Therefore, it is an excellent approach for combating damage arising from water droplet erosion of LPST blades.

The fracture toughness of the advanced HVOF coating appears to be much higher than in the conventional HVOF coatings. This may be another reason of its enhanced droplet erosion resistance.

The grain morphology of 17Cr-4Ni PH is the finest of all the materials tested. This may be one reason for its enhanced droplet erosion and corrosion resistance compared with X10CrNiMoV122 and X20Cr13 steels.

The 17Cr-4Ni PH and X10CrNiMoV122 steels have been shown to perform better than X20Cr13 steel in salt spray tests. The droplet erosion resistance of these steels is also much better than X20Cr13 steel. These steels also possess better mechanical strength than X20Cr13 steel, and so can be used for LPST blading.

Acknowledgments

The authors are thankful to Dr. C.R.K. Prasad and Dr. N. Mukhopadhyay for their useful discussions on this subject. Thanks are also due to Mr. M.K.V.H. Sarma for his help in reducing the vibration in the droplet erosion test facility. The

Fig. 12 Droplet eroded LPST blades of 60 MW steam turbine after 15 years of operation

authors are also thankful to the management of BHEL, Corporate R&D, Hyderabad, India, for permission to publish this paper.

References

1. "Erosion by Cavitation or Impingement," F.J. Heymann, Ed., ASTM STP 408, *Annual Book of ASTM Standards,* ASTM, 1967, p 3-158
2. W.F. Adler, The Mechanics of Liquid Impact Treatise on Materials Science and Technology, Vol 16, 1979, p 127-183
3. J. Krzyzanowski, The Correlation Between Droplet Steam Structure and Steam Turbine Blading Erosion, *J. Eng. Power,* July, Vol 96, (No. 3) 1974, p 256-266
4. J. Krzyzanowski and Z. Szperngiel, The Influence of Droplet Size on the Turbine Blading Erosion Hazard, *J. Eng. Power,* Vol 100, October, 1978, p 561-565
5. "Standard for Liquid Impingement Erosion Testing," ASTM-G73-82 Vol 03.02, *Annual Book of ASTM Standards,* ASTM
6. "Erosion, Prevention and Useful Application," W.F. Adler, Ed., ASTM STP 664, 1979, p 3-615
7. Treatise on Materials Science and Technology, Vol 16, *Erosion,* C.M. Preece, Ed., Academic Press, New York, 1979
8. "Characteristics and Determination of Erosion Resistance," A. Thirunengadam, Ed., ASTM STP 474, 1970, p 3-434
9. J.H. Brunton, Deformation of Solids by Impact of Liquids at High Speeds, Vol 03.02, ASTM STP 307, *Annual Book of ASTM Standards,* ASTM, 1962, p 83-98
10. B.S. Mann and V. Arya, HVOF Coating and Surface Treatment for Enhancing Droplet Erosion Resistance for Steam Turbine Blades, *Wear,* Vol 254, 2003, p 652-667
11. J. Grum and R. Sturm, Residual Stresses State after the Laser Surface Remelting Process, *J. Mater. Eng. Perf.,* Vol 10 (No. 3), 2001, p 270-281
12. J. Grum and R. Sturm, Deformation of Specimens During Laser Surface Remelting, *J. Mater. Eng. Perf.,* Vol 9 (No. 2), 2000, p 138-146
13. J. Grum and R. Sturm, Influence of Laser Surface Melt Hardening Conditions on Residual Stresses in Thin Plates, *Surf. Coat. Technol.,* Vol 100-101, 1998, p 455-458
14. S. Kuroda, Y. Tashiro, H. Yumoto, S. Taira, H. Fukanuma, and S. Toge, Peening Action and Residual Stresses in High Velocity Oxygen Fuel Thermal Spraying of 316 Stainless Steel, *J. Therm. Spray Technol.,* Vol 10 (No. 2), 2001, p 367-374
15. D. Cooper, F.A. Davis, and R.K.J. Wood, Selection of Wear Resistant Materials for the Petrochemical Industry, *J. Phys. D: Appl Phys.,* Vol 25, 1992, p A195-A204
16. "Standard Method of Salt Spray (Fog) Testing," Vol 03.02, ASTM B 117-73 (Reproved 1979), *Annual Book of ASTM Standards,* ASTM, p 31-37
17. S. DePalo, M. Mohanty, H. Marc-Charles, and M. Dorfman, Thermal Spray: Surface Engineering via Applications, Vol 5, 2000, p 245-250
18. H.L. de Villers Lovelock, Powder/Processing/Structure Relationship in WC-CO Thermal Spray Coatings: A Review of Published Literature, *J. Therm. Spray Technol.,* Vol 7 (No. 3), 1998, p 357-373
19. F.J. Heymann, Conclusions from the ASTM Inter Laboratory Test Programme with Liquid Impact Erosion Facilities, J.E. Field, Ed., *Proceedings of the 5th International Conference on Erosion by Liquid and Solid Impact*, September 3-6, 1979, Cavendish Laboratory, University of Cambridge, Cambridge, UK, 1979
20. H.G. Feller and Y. Kharrazi, Cavitation Erosion of Metal and Alloys, *Wear,* Vol 93, 1984, p 240-260
21. N. Frees, Cavitation Erosion of Titanium Carbide Coatings on Cemented Carbide and Other Substrates, *Wear,* Vol 88, 1983, p 57-74